INSTITUTE OF PHYSICS PUBLISHING JOURNAL OF PHYSICS D: APPLIED PHYSICS

J. Phys. D: Appl. Phys. **39** (2006) 4450–4456 doi:10.1088/0022-3727/39/20/023

Real time observation of dendritic solidification in alloys by synchrotron microradiography

B Li[1], H D Brody[1], D R Black[2], H E Burdette[2] and C Rau[3]

[1]Department of Metallurgy and Materials Engineering, University of Connecticut, Storrs, CT 06269-3136, USA
[2] National Institute of Standards and Technology, Gaithersburg, MD 20899, USA
[3] Frederick-Seitz Materials Research Laboratory, University of Illinois at Urbana Champaign, Argonne, IL 60439, USA

Received 29 December 2005, in final form 16 July 2006
Published 29 September 2006
Online at stacks.iop.org/JPhysD/39/4450

Abstract
A third generation synchrotron x-ray source and advanced imaging facilities were used to study dendritic solidification in metallic alloys in real time. A digital camera and a video camera with different time and spatial resolution were tested to capture growing dendrites during solidification of Sn–13 wt%Bi and Al–25 wt%Cu alloys. The captured digital images show that the morphology of the dendrites can be resolved with satisfactory resolution and contrast. The trade-off between spatial resolution and time resolution was discussed. The effect of beam characteristics such as intensity, parallelism and coherency on both spatial and time resolution was analysed, and potential improvements with higher image quality with reduced exposure time were also discussed.

1. Introduction

To unambiguously understand alloy solidification processes requires direct observations of the growth of solid phases in the melt, which is normally invisible for real alloys due to their opacity. Though indirect observation techniques [1, 2] such as interface quenching have provided valuable insights towards understanding alloy solidification, these techniques cannot observe detailed information of dendrite growth and solute redistribution during the solidification of real alloys in real time. For instance, in interface quenching [1, 2], solidification is interrupted by quenching a solidifying sample at the mushy temperatures. The remaining liquid rapidly solidifies into a fine structure, and the primary solid phase can be easily distinguished from the liquid when morphological observations and quantitative measurements are performed on polished surfaces of the sample. One disadvantage in these observations is that any information about microstructural evolution before the quenching is lost. For direct observations of solidification in transparent alloy analogues, there is a significant difference between their thermal and physical properties and that of real alloys [3–6]. Therefore, direct observation in real time of real alloys is preferred in order to achieve better understanding of alloy solidification.

The high penetrating power of hard x-rays (energy above 10 keV) has made microradiography unique in observing internal structures of metallic materials [7–12]. Among the applications of microradiography is real time observation of alloy solidification [10–12]. Early observations were limited by the characteristics of available x-ray sources, such as intensity and divergence, and images were captured with limited resolution and contrast and only qualitative results were obtained [10–12]. More recently, advances in technology such as digital cameras coupled with solid-state imaging detectors that have fast response to x-ray photons and new types of x-ray sources have stimulated renewed interest in real time studies of alloy solidification [13–17].

Despite the fact that more and more data have been collected by the microradiography technique in studies of alloy solidification [13–17], carrying out such experiments is somewhat difficult, in the sense that capturing high quality images is elusive. By quality we mean image contrast and resolution. To well resolve features of the growing solid phase in the melt of real alloys requires comprehensive knowledge of x-ray optics, alloy solidification and modern imaging technology. Not surprisingly, most previous observations were qualitative due to the limited image quality. To attain

quantitative analyses based on real time observations, higher image quality has to be achieved.

In earlier experiments, dendrite coarsening and temperature gradient zone melting (TGZM) in an Sn–13 wt%Bi alloy were studied using synchrotron radiation at the Cornell High Energy Synchrotron Source (CHESS) [18, 19]. In these experiments, an x-ray optical system combined with a high resolving power negative film was used to capture growing dendrites with an exposure time of a fraction of a second (typically below 0.1 s). Positive images were then developed in the darkroom. Quantitative data of dendrite coarsening and rate of TGZM in directional solidification were obtained [18, 19]. Despite the high image quality in terms of spatial resolution and contrast, the photographic development of images is laborious and time consuming and the need to place the film in the experimental enclosure limits temporal resolution. A real time digital imaging system, of comparable image quality, is more convenient and can easily identify the beginning of the dendrite growth. In the present paper, we describe an imaging system utilizing a third generation synchrotron radiation source, the Advanced Photon Source (APS), Argonne National Laboratory (ANL) and advanced digital camera systems, that provides improved image quality compared with previous results. We apply this system to the real time study of alloy solidification in Sn–Bi and Al–Cu alloys.

2. Experimental method

When x-rays pass through a solidifying alloy sample, image contrast can be produced from several sources. One is the density difference between the solid and the liquid, which is usually negligible. Another is the phase contrast that is produced when a coherent x-ray beam refracts from structures within the sample with different indices of refraction. This kind of contrast has potential applications in imaging structures that only have small absorption contrast [20]. The major source of image contrast comes from the composition difference between the solid and the liquid. During cooling in alloy solidification, if we assume the solid is in equilibrium with the liquid, then the liquid composition follows the liquidus line, and the solid composition follows the solidus line in an equilibrium phase diagram. Thus, the solute partition ratio k, defined as the ratio between the solid composition and the liquid composition, plays an important role in the image contrast. For a eutectic alloy with $k < 1$, during solidification, the first formed solid is purer in a solute, and the solute has to be rejected into the liquid, which is therefore enriched with the solute. This important feature of solute redistribution in alloy solidification produces the image contrast that is necessary to distinguish the solid from the liquid. Hence, larger differences in the absorption coefficients between the alloying elements, relatively higher nominal composition and smaller partition ratio k, are preferred in order to capture high quality images of the growing solid. In this work, Sn–13 wt%Bi and Al–25 wt%Cu alloys were used to observe dendritic solidification in real time.

Both Sn–13 wt%Bi and Al–25 wt%Cu alloys are hypoeutectic, with a eutectic point of (57 wt%Bi, 139 °C) and (33 wt%Cu, 548 °C), freezing range (from liquidus to eutectic temperature) of 75 °C and 28 °C, respectively. The absolute

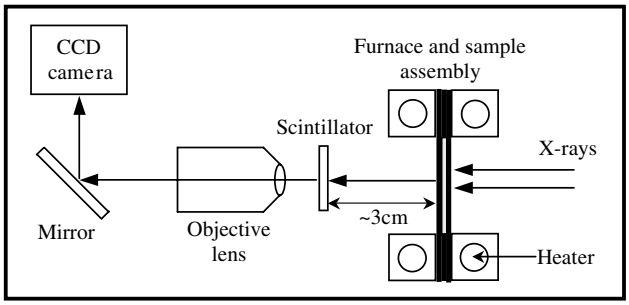

Figure 1. Schematic of experimental setup. The distance between the scintillator and the sample was roughly 3 cm. The objective lens was focused on the scintillator. The temperature gradient (G) on the sample could be upwards or downwards. In this work, G was always upwards (against the gravity) in order to minimize thermally driven convection.

difference in absorption coefficients between Sn and Bi, Al and Cu is relatively large, and accordingly the Sn–Bi and Al–Cu alloys have often been used in microradiography studies [13,15,17–19].

Figure 1 shows schematically the experimental setup on the bending magnet line of sector 33-(UNICAT) of the APS. The setup was composed of a solidification furnace and an imaging system. The furnace was made up of two identical, separable heaters that reside on the top and bottom of the furnace, providing the desired temperature control. The cooling rate (ε) and the temperature gradient (G) were adjustable through programmable temperature controllers. Cooling rates with sufficient linearity and thus steady state growth can be achieved.

A thin (typically 130 $\sim$ 150 μm in thickness), well-polished solid sample was sandwiched and sealed between two graphite plates, and the sample assembly was fixed between the top and the bottom heaters. Graphite was used because it has good heat conductivity and is almost transparent to the x-rays. Hence, intensity attenuation after the x-rays pass through the sample assembly was mainly caused by the metallic sample. In the case of Al–Cu samples, due to the much higher liquidus temperature than the Sn–Bi alloy, the surfaces of the graphite were coated with a thin layer of BN in order to slow down oxidation at elevated temperatures. The total thickness of the graphite walls was about 1.2 $\sim$ 1.5 mm.

The temperature control scheme in this work was such that the sample stayed still during solidification, but the temperature was decreased linearly in a well controlled fashion. The actual temperature of the sample was measured by two thermocouples 10.0 mm apart and directly attached to the sample. A more detailed description of the construction of the furnace and the graphite crucible, temperature control and measurement was provided elsewhere [21].

As shown in figure 1, after the x-rays passed through a solidifying sample, the absorption image of the sample was recorded by the detector and the camera. The detector contained a scintillation crystal, which transformed the impinging x-rays into visible light. A 5× object lens was focused on the scintillation screen. The detector, the sample and the x-ray beam were carefully aligned before experiments, so that one of the thermocouple beads was seen in the field view and served as a good reference point for quantitative

measurements. The image formed on the scintillator was then projected onto the chip of a CCD camera via the optical microscope and then stored as digital information on a computer hard drive. For the experiments we used a high dynamic range (typically 14-bit), high signal-to-noise-ratio Kodak KX2e camera with a 1536 × 1024 pixel array and $9 \times 9\,\mu\,\mathrm{m}^2$ size of each Pixel. The scintillation screen was a 150 μm-thick yttrium alumina garnet single crystal with a 26 μm europium doped layer.

An infinity-corrected objective lens with a long working distance was used. For the 5× magnification the working distance is 34 mm and the numerical aperture is 0.14. A tube lens with 1× magnification is placed directly behind the objective lens to form a real image on the CCD chip of the camera 240 mm away. Using a 5× objective lens and 2 × 2 binning of the camera, the effective size of each pixel on the scintillation screen is 3.6 μm. Typical exposure times are in the order of a couple of seconds.

The x-ray beam was slit down to about 5 × 4 mm for real time observations. The photon energy for the Al–25 wt%Cu and Sn–13 wt%Bi alloys was 13 KeV and 20 KeV, respectively. Though theoretically the best image contrast could be achieved when photon energy was chosen near the absorption edges of the elements, experimental results showed that photon energy slightly away from the absorption edges to the high end offered better efficiency in the optics.

3. Results and discussion

Figure 2 shows digital images captured in the experiments. All the images presented are original without any image enhancement. Figures 2(*a*)–(*c*) are the images of growing dendrites in the Sn–13 wt%Bi alloy when the sample was directionally solidified at a cooling rate $\varepsilon = 2^\circ\,\mathrm{C\,min^{-1}}$ and temperature gradient $G = 10^\circ\,\mathrm{C\,cm^{-1}}$, corresponding to a local solidification time 2250 s. Each image was integrated over 3 s. In this scenario, the dendrites popped out across the whole field of view quickly (figure 2(*a*)). At first glance, the 'primary' dendrite arms look like they were growing along the temperature gradient, with secondary arms branching to both sides of the 'primary' arms. However, a closer look at the dendritic structure reveals that the 'primary' arms were actually made up of well aligned, separate segments of short arms, as schematically shown in the lower-left corner of the field of view. Each segment conjoined two other branches and formed a triplet. Such a growth pattern is very different from the normal, directionally solidified dendritic structure. Figure 2(*b*) was captured 66 s after figure 2(*a*) and we can clearly see that dendrite coarsening was happening. Each branch of the triplets grew rounder and fatter, turning each triplet into a short solid band. At this time, a structure of alternating solid and liquid bands was formed. Figure 2(*c*) is an image of the dendrites at the later stage of solidification, 312 s after figure 2(*a*). Compared with figure 2(*b*), dendrites are coarser, and coarsening by coalescence can be clearly seen. Neighbouring solid bands interconnected and eventually coalesced.

Each frame shown in figure 2 integrates over 3 s during imaging, in order to accumulate sufficient intensity to achieve better image quality in terms of contrast and resolution. Under these growth conditions, the dendrite tips were moving at a rate of about 33 $\mu\mathrm{m\,s^{-1}}$ and the images of the moving tips would be blurred with such a long exposure time. Because the thickening and coarsening rates of the side arms are much slower than the growth rate at the tips, this exposure is acceptable for imaging the growth of side arms behind the growth front. In the study of alloy solidification, solute redistribution around the growing tips is of most interest, in the sense that features such as interface instability and microsegregation are closely associated with solute redistribution. In order to capture moving dendrite tips with reasonable resolution, exposure time has to be reduced.

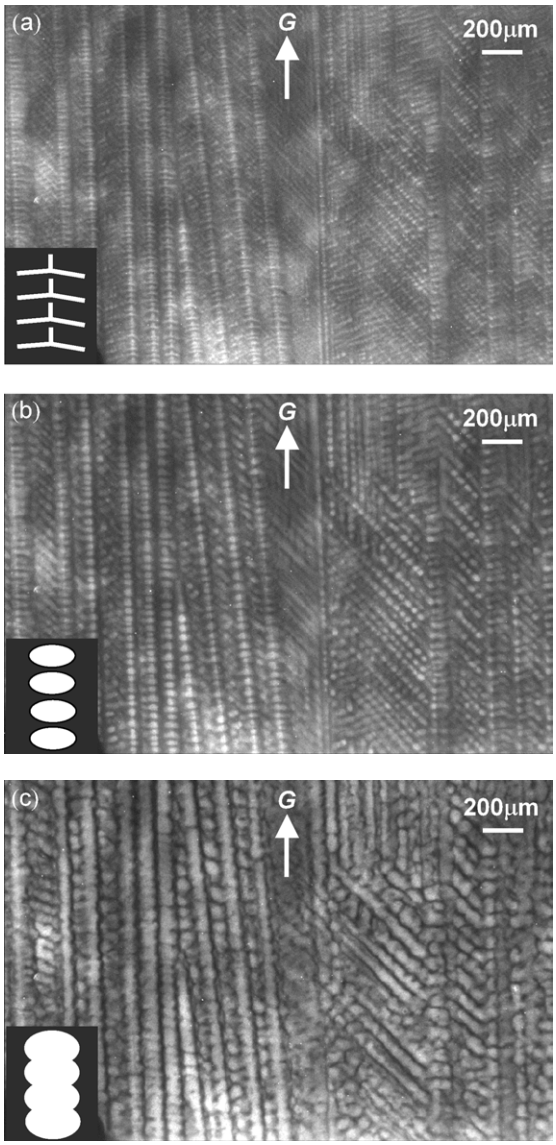

Figure 2. Transverse growth pattern in the Sn–13 wt% Bi alloy captured by the digital camera, each frame is integrated over 3 s. The cooling rate $\varepsilon = 2^\circ\,\mathrm{C\,min^{-1}}$ and the temperature gradient $G = 10^\circ\,\mathrm{C\,cm^{-1}}$ (G was upwards), corresponding to a local solidification time 2250 s. The dendrites (solid phase) were purer in solute (Bi) than the liquid due to the solute partitioning and hence were less absorptive and looked brighter. (*a*) Transverse growth pattern with fine dendrites, (*b*) 66 s after (*a*), dendrite coarsening can be seen. The solid triplets became separate, solid bands, (*c*) 312 s after (*a*). The solid bands interconnected by coalescence.

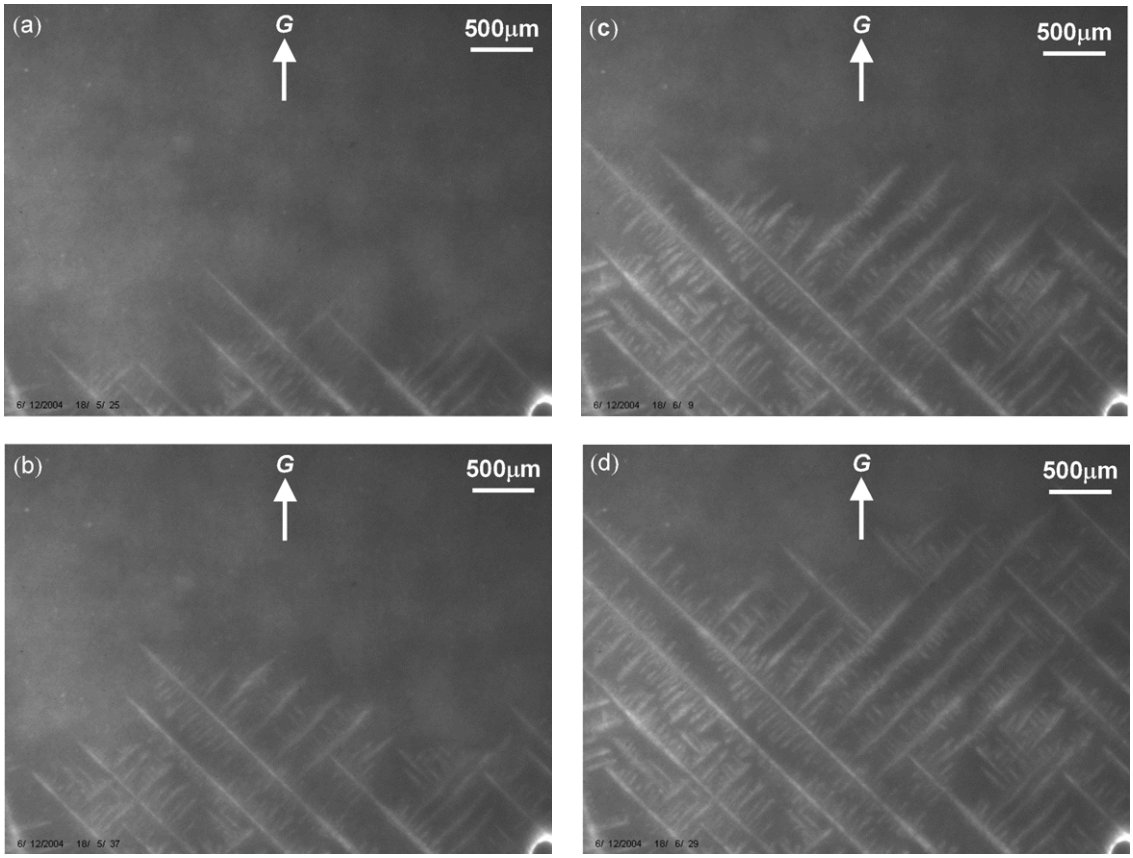

Figure 3. Longitudinal growth pattern captured by the real time camera. Each frame was averaged over 0.3 s. Cooling rate $\varepsilon = 2^\circ\,\mathrm{C\,min^{-1}}$ and temperature gradient $G = 10^\circ\,\mathrm{C\,cm^{-1}}$. Solute enrichment in the mushy zone can be recognized. Dendrite selection can be seen. The black dot on the lower right corner was the thermocouple bead. (*a*) Longitudinal growth pattern, (*b*) 12 s after (*a*), (*c*) 44 s after (*a*) and (*d*) 64 s after (*a*).

A real time x-ray sensitive video camera with much faster read-out rate was then used to replace the digital camera, in order to achieve faster data acquisition. The camera has a 3 : 4 image aspect ratio and a 5.5 mm diagonal CCD chip with 768 × 494 6.5 μm pixels. The overall image resolution is better than 10 μm. A scintillation coated fibre optic is coupled directly to the CCD chip. A frame grabber was used to capture digital images. The grabber could capture 30 frames every second at full speed and allow on-chip image processing such as integrating, averaging or summing over a certain number of frames. Digital frames were then dumped in the computer storage.

The change from the digital camera to the real time camera sacrificed the overall image resolution, but significantly reduced the exposure time. With the installation of the real time camera and the image grabber, integration over the first 10 of the 30 frames of each second resulted in a much shorter exposure time of about 0.3 s, and the growing dendrite tips could be resolved under the applied growth condition in this work.

Figure 3 shows digital images of growing dendrites in the Sn–13 wt%Bi alloy captured by the real time camera. The frames were organized in time sequence. The growth condition was the same as in figure 2. Compared with the growth pattern in figure 2, the dendritic structure in this scenario was much different, in that the dendrites took a well-defined, normal dendritic morphology. Sharp dendrite tips can be easily recognized. The primary arms were growing upwards, at an angle of about 45° with respect to the temperature gradient. Dendrite selection can be seen during solidification. Some primary arms were stopped when they impinged upon the secondary arms protruding in front (figure 3(*c*)). In the mean time, some tertiary arms were developing into primary arms and reduced the primary dendrite arm spacing (figure 3(*b*)).

Another important feature we can see from figure 3 is that the interdendritic regions (mushy zone) look darker than the liquid zone above the growth front. As expected, these regions were enriched with solute (Bi) and, consequently, more absorptive. Within a small layer in front of the growing dendrite tips, a solute boundary layer can be recognized as a result of the solute being rejected into the liquid. Solute redistribution is well known, but it is very difficult to quantitatively measure the liquid concentration during alloy solidification [22]. Real time microradiography of dendritic solidification in real alloys provides the possibility of measuring solute partitioning during solidification. Mathiesen and Arnberg [15] have tried to extract a liquid composition profile from digital images.

The band structure obtained in figure 2 results from transverse growth of dendrites in thin samples, while the dendritic structure shown in figure 3 results from normal, longitudinal growth of dendrites. Figure 4 shows an image of dendrites taken by contact microradiography. A thin, solid sample taken from a directionally solidified ingot was imaged.

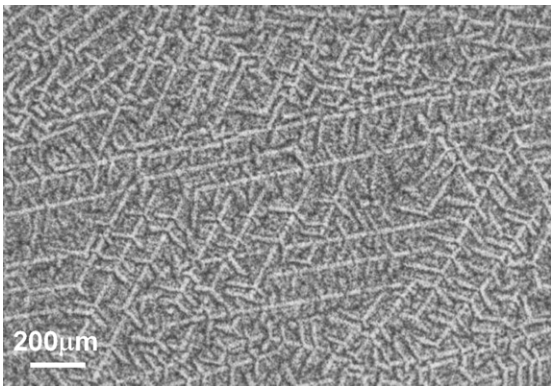

Figure 4. Image of a dendrite structure of a solid Sn–13 wt%Bi sample by contact microradiography. The image was taken on a transverse section of a directionally solidified ingot. The plane of view is perpendicular to the temperature gradient. The triplets were similar to that of figure 2(*a*).

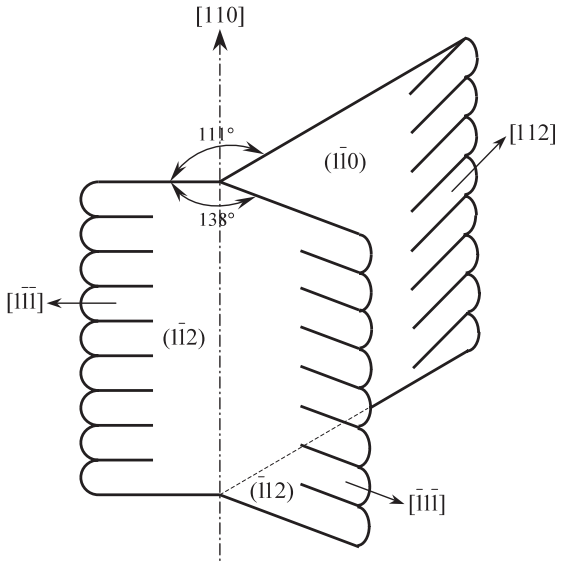

Figure 5. Schematic diagram showing the crystallographic structure of a dendrite in an Sn–Bi alloy (adapted from [23]). If we look at the dendrites against the [110] direction, then a transverse pattern of triplets in figures 2(*a*) and 4 can be seen. If we look at the dendrites from the direction perpendicular to the paper plane, then a longitudinal pattern in figure 3 can be seen.

The plane of view is perpendicular to the temperature gradient. If we compare figure 4 with figure 2(*a*), we can easily see these two structures are similar, in the sense that they both consist of separate dendrite triplets. Figure 4 confirms that the pattern in figure 2(*a*) originated from transverse growth. This can be further understood from figure 5, which shows schematically the 3D structure of a dendrite in Sn–Bi alloys [23]. In figure 5, if we look at the dendrites against the [110] direction, then a transverse pattern of triplets in figures 2(*a*) and 4 can be seen. If we look at the dendrites from the direction perpendicular to the paper plane, then a longitudinal pattern in figure 3 can be seen. The preferred growth direction is [110] in a regular pattern. When the [110] direction is roughly along the temperature gradient, the longitudinal pattern in figure 3 will be obtained. In the case of thin samples, the preferred growth direction [110] might be diverted to the direction of sample thickness (orthogonal to the temperature gradient), which is along the x-ray beam, due to the thermal fluctuation in the transverse direction. Because the graphite crucible was sandwiched between two brass blocks, minor temperature difference in the transverse direction could result in an appreciable temperature gradient on the thin metallic sample. The mechanism of dendrite growth selection between transverse and longitudinal is worth future investigation.

Figure 6 shows digital images of growing dendrites in the Al–25 wt%Cu alloy. The cooling rate ε was 2.0 °C min^{-1} with a negligible temperature gradient. Local solidification time in this case was 840 s. We can see that equiaxed grains nucleated in the melt. Interestingly, as soon as these grains were formed, they quickly floated to the top of the sample. This indicates that the solid is less dense than the liquid because the liquid was enriched with Cu. This is consistent with the observations from Mathiesen *et al* [13]

As we can see from the quality of the digital images, the application of the advanced microradiographic technique to observe dendritic solidification in real time in real alloys is encouraging and promising. However, under the given experimental conditions, the constraints of absorption contrast and available intensity and the consequential limitation on both temporal and spatial resolution have become obvious.

In principle, the x-ray imaging system can be configured for imaging with micrometre resolution, but in practice the actual resolution achievable when imaging a mixture of solid and liquid in real samples is limited by several factors. The efficiency of the CCD detector system decreases strongly with increasing resolution, due to the fact that the high spatial resolution is achieved by a thinner and thus less efficient doped layer of the scintillation screen. In addition the number of photons per CCD-pixel decreases. As a result the exposure times increase and limit time resolved imaging.

The second difficulty comes from the weak absorption contrast of the features in the early stage of the growth of dendrites. When the growing dendrites reach a size comparable to the spatial resolution of the imaging system we would anticipate that they could be resolved. But this is not the case due to the statistical nature of image quanta. If a feature with a given contrast C can be detected, it is given by the rose signal-to-noise ratio $\Delta SNR_{\mathrm{Rose}} = C\sqrt{A \cdot q_{\mathrm{b}}}$, where A is the area over which the number of photons is integrated and q_{b} the average number of photons per area. The value of the rose signal-to-noise ratio should be at least 5 so that a feature can be detected. For small (thin) objects and small contrast the number of photons has to be increased by the square to detect the structure. Consequently, it is not just the spatial resolution that will determine if a feature can be resolved. If the magnitude of the contrast between regions that contain both solid and liquid and surrounding regions of 100% liquid is not sufficiently large (typically a few per cent) for the detector, then the dendrites will not be resolved in the imaging system, even though their size already grows above the physical resolution of the optics. This resolvable contrast is related to the nominal composition of the alloy, the absolute difference in the absorption coefficients of the alloy elements and the equilibrium partition ratio.

Additional limitations on the image resolution come from the divergence of the x-ray beam, which produces geometrical

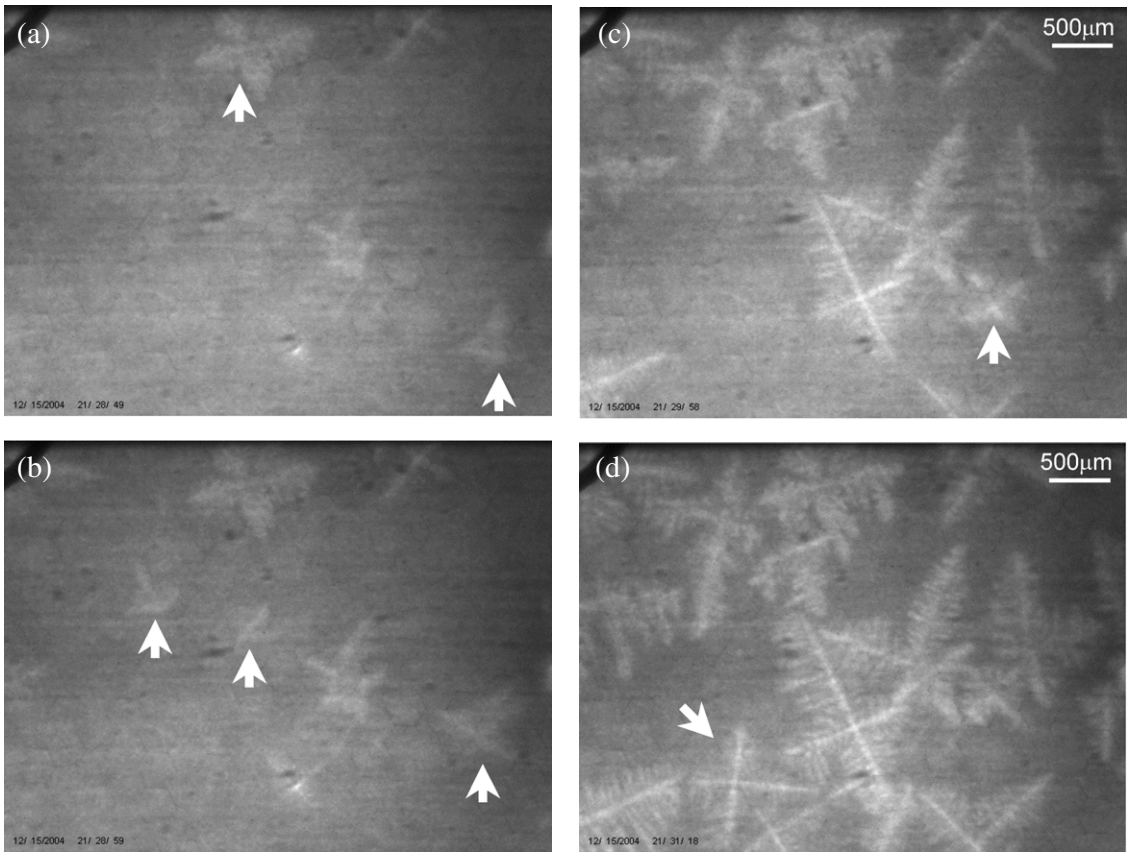

Figure 6. Nucleation and floatation of dendrites in the Al–25%Cu alloy captured by the real time camera. Each frame sums over 0.3 s. Cooling rate $\varepsilon = 2^{\circ}\,\mathrm{C\,min^{-1}}$ and negligible. As indicated by the arrows, dendrites floated to the top of the sample due to buoyancy. Part of the thermocouple wire can be seen in the left upper corner. The local solidification time was about 840 s. (*a*) Equiaxed grains formed in the Al–25 wt%Cu alloy, (*b*) 10 s after. Dendrites floated after formation, (*c*) 69 s after (*a*) and (*d*) 149 s after (*a*).

image unsharpening which worsens as sample-to-detector distance is increased. For this consideration, the sample-to-detector distance has to be as small as possible when microradiography experiments are conducted at the bending magnet beamline. However, the risk that the detector becomes heated up exists because the sample temperature is high. Measures have to be taken to keep the detector cool, and this generates difficulty in reducing the sample-to-detector distance. Other limitations include image blurring from moving the solid–liquid interface. Such blurring deteriorates when the growth rate is increased.

During alloy solidification, features of dendrites are usually of the order of tens of microns. However, the early stage of dendrite growth with finer features is of most interest to metallurgists. As a consequence, any improvement in resolution, both spatial and temporal, would help significantly in the understanding of the growth process. To overcome the limitations discussed above, we seek an undulator beamline with higher intensity, better parallelism and beam coherence.

Much shorter exposure times may be achieved at an undulator beamline using the so-called 'pink beam' [20]. The undulator is one type of insertion device, producing a series of narrow peaks in the energy spectrum. The radiation is very intense, emitted in a small horizontal and vertical angle, if compared with those coming from a bending magnet. The source size at the undulator beamline 34 ID is $600\,\mu$m $\times$ $40\,\mu$m (horizontal $\times$ vertical) and the beam divergence is $40\,\mu$rad $\times$ $12\,\mu$rad (horizontal $\times$ vertical). A silicon mirror with differently coated stripes deflects the beam to the hutch. The coating and deflection angle define the cutoff energy. At a deflection angle of 5 mrad and choosing platinum coating, radiation above 15 KeV is rejected. The fixed-exit double crystal monochromator is water cooled and yields an energy bandwidth of $\Delta E/E = 10^{-4}$ using silicon (111) crystals over an energy range 6–30 KeV. Without using the monochromator a single undulator harmonic can be filtered by the reflecting mirror together with air absorption or an absorption filter acting as a bandpass filter. In this case, the flux is 50–100 times more intense. The latter configuration is called the 'pink beam'. In addition to the higher intensity, the detector can be configured for imaging with micron resolution. Extra contrast can be gained when imaging features with small absorption contrast, and image quality can be improved with in-line phase contrast imaging, taking advantage of the highly coherent radiation available at an undulator beamline [13].

We have made preliminary tests at an undulator beamline with monochromatic illumination of the samples, achieving faster exposure times with finer spatial resolution. Using a monochromatic beam, a photon energy of about 9 KeV (for Al–Cu alloy) and a distance of 55 mm from the experimental table to the source, we achieved a slightly oval beam size around 1 mm^2 and photon flux $10^{13}\,\mathrm{s^{-1}}$. The beam size was significantly decreased in this case, but still large enough for imaging dendrites typically sized around tens of microns. The

continuation of this study with increased resolution and shorter exposure would be of great interest. We will report the results afterwards.

4. Conclusions

We present qualitative observations of dendritic solidification in real time in real alloys using an advanced microradiographic technique, and the results are promising. The image quality is satisfactory in terms of the image contrast and resolution. A transverse growth pattern was observed in the thin Sn–13 wt%Bi samples. Solute enrichment in the mushy zone can be recognized. Floatation of solid in the liquid in the Al–25 wt%Cu alloy was observed, indicating that the solid is less dense than the liquid. This technique can be applied to study a variety of phenomena in alloy solidification such as solute redistribution within diffusion distance around dendrite tips and structure formation and will help clarify mysteries in otherwise invisible processes of alloy casting and solidification.

Acknowledgments

The UNICAT facility at the APS is supported by the US DOE under Award No DEFG02-91ER45439, through the Frederick Seitz Materials Research Laboratory at the University of Illinois at Urbana-Champaign, the Oak Ridge National Laboratory (US DOE contract DE-AC05-00OR22725 with UT-Battelle LLC), the National Institute of Standards and Technology (US Department of Commerce) and UOP LLC. The APS is supported by the US DOE, Basic Energy Sciences, Office of Science, under contract No W-31-109-ENG-38.

References

[1] Kattamis T Z, Coughlin J C and Flemings M C 1967 *Trans. AIME* **239** 1504
[2] Young K P and Kirkwood D H 1975 *Metall. Trans.* A **6** 197
[3] Kahlweit M 1968 *Scr. Metall.* **2** 251
[4] Marsh S P and Glicksman M E 1996 *Metall. Trans.* A **27** 557
[5] Glicksman M E and Schaefer R J 1966 *Acta Metall.* **14** 1126
[6] Jackson K A and Hunt J D 1965 *Acta Metall.* **13** 1212
[7] Tzavaras A A and Flemings M C 1965 *AIME Trans.* **233** 355
[8] McLean M 1973 *Phil. Mag.* **27** 1253
[9] Boettinger W J, Voorhees P W, Dobbyn R C and Burdette H E 1987 *Metall. Trans.* A **18** 487
[10] Miller E W J and Beech J 1972 In-situ radiographic observations of alloy solidification *Metallography* **5** 298
[11] Curreri P A and Kaukler W F 1996 *Metall. Trans.* A **27** 801
[12] Sen S, Kaukler W F, Curreri P and Stefanescu D M 1997 *Metall. Trans.* A **28** 2129
[13] Mathiesen R H, Arnberg L, Ramsoskar K, Weitkamp T, Rau C and Snigirev A 2002 *Metall. Trans.* B **33** 613
[14] Mathiesen R H, Arnberg L, Mo F, Weitkamp T and Snigirev A 1999 *Phys. Rev. Lett.* **83** 5062
[15] Mathiesen R H and Arnberg L 2005 *Acta Mater.* **53** 947
[16] Thi H N *et al* 2003 *J. Phys. D: Appl. Phys* **36** A83
[17] Yasuda H *et al* 2004 *J. Cryst. Growth*. **262** 645
[18] Li B, Brody H D and Kazimirov A 2004 *Phys. Rev.* E **70** 062602
[19] Li B, Brody H D and Kazimirov A 2006 *Metall. Trans.* A **37** 1039
[20] Rau C, Weitkamp T, Snigirev A, Schroer C G, Benner B, Kuhlmann M and Lengeler B 2002 Hard X-ray tomography with high resolution *Developments in X-ray Tomography III* ed U Bonse *Proc. SPIE* **4503** 14–22
[21] Li B, Brody H D, Black D R, Burdette H E and Rau C 2006 *Meas. Sci. Technol*. **17** 1883
[22] Brody H D and Flemings M C 1966 *Trans. AIME* **263** 615
[23] Ahearn P J and Flemings M C 1967 *Trans. AIME* **239** 1590